Continuum Mech. Thermodyn. (2009) 20: 509–521
DOI 10.1007/s00161-008-0090-0

ORIGINAL ARTICLE

Maxim A. Zapara · Nikolay D. Tutyshkin · Wolfgang H. Müller · Kerstin Weinberg · Ralf Wille

A physico-mechanical approach to modeling of metal forming processes—Part II: damage analysis in processes with plastic flow of metals

Received: 13 November 2007 / Accepted: 20 November 2008 / Published online: 23 January 2009

Abstract A damage analysis is presented for the extrusion of a case-shaped cylindrical part by using a physico-mechanical approach for modeling metal forming processes. Two integral measures related to the hydrostatic and deviatoric parts of the damage tensor are used for the calculation of strain damage. The combined use of *two* damage measures in contrast to only one allows us to assess not only a risk of macro-fracture of the deformed material but also the stage of formation of large cavernous defects due to coalescence of ellipsoidal voids. Such a refined prediction of the actual quality of the material's micro-structure is important when producing metalware that is supposed to operate under intense loading and thermal conditions. In case study of this paper the kinetic equations of damage are solved by using mutually consistent fields of stresses, flow velocities, and strains. It is shown that the predicted damage is less than its permissible value since a high hydrostatic pressure in the plastic zone heals the micro-defects, prevents their growth, and, thereby, increases the processing ductility of deformed metals during extrusion.

Keywords Plasticity · Plastic flow · Deformation · Plastic strain and stress · Slip line · Velocity field · Micro-structure · Strain induced damage · Meso-parameters · Damage equation · Metal forming · Extrusion · Case-shaped part

PACS 81.40.Lm · 81.20.Hy · 46.35.+z · 46.50.+a · 62.20.F– · 61.72.Qq

1 Introduction

The physico-mechanical approach to modeling Metal Forming (MF) processes as developed in Part I of this paper [21] is now applied to the analysis of a process with axisymmetric plastic flow. The constitutive equations describing large plastic deformations under complex loading (with changeable Lode angle) are based on both plastic flow theory as well as damage mechanics. The definition offered for the symmetric second-rank

Communicated by S. Seelecke

M. A. Zapara · N. D. Tutyshkin
Department of Technological Mechanics, Tula State University,
300600 Tula, Russia

W. H. Müller (✉) · R. Wille
Lehrstuhl für Kontinuumsmechanik und Materialtheorie,
Technische Universität Berlin, Sekretariat MS 02, Einsteinufer 5,
10587 Berlin, Germany
E-mail: Wolfgang.H.Mueller@tu-berlin.de

K. Weinberg
Universität Siegen, Fachbereich 11, Maschinenbau, Paul-Bonatz-Strasse 9-11,
57076 Siegen, Germany

order tensor of damage is physically motivated since its hydrostatic and deviatoric parts describe the evolution of damage connected with a change in volume and with the shape of the micro-defects, respectively. Consequently, this representation of damage kinetics requires us to use two integral measures (ω_1 and ω_2) for the calculation of damage in deformed materials: The measure ω_1 determines plastic dilatation related to an increase in void volume. It allows for a quantitative assessment of the risk of metal fracture caused by a critical amount of plastic dilatation ($\varepsilon^{i}_{\cdot i_{cr}}$). In physical terms the measure ω_1 is identically equal to the measure ω in dissipative damage theory [6] and is connected with the void volume fraction (f_v) that is used as damage measure in some models [3,12,13]. The measure ω_2 accounts for the deviatoric strain of voids which is connected with a change in their shape ($\widehat{\boldsymbol{e}}$). The critical deformation of ellipsoidal voids corresponds to their intense coalescence and to the formation of large cavernous defects. It was demonstrated experimentally that the shape of the voids strongly effects their coalescence and, consequently, the formation of cavities in deformed material [4,8,11]. The critical deformation of ellipsoidal voids ($\widehat{\boldsymbol{e}}_{cr}$) corresponds to their intense coalescence and to the formation of large cavernous defects. Thus, we may say that the measure ω_2 assesses a risk of material microfracture at the mesolevel. The use of ω_2 is advantageous when producing metalware that is required to operate under intense loading and thermal actions, high pressures and strain rates. Such products and components are generally used in aerospace, automotive, and energy engineering.

Many complicated problems in research and development of MF techniques are still insufficiently investigated for products with irregular shape. In particular, for extrusion, where the processed material is under complex loading with strong variations of the stress state, it is very difficult to analyze and optimize the full process. The choice of an extrusion process for the case study of this paper is explained by its wide use in MF. The compressive regime of the stress state during extrusion promotes high ductility of the processed materials and, accordingly, a greater operational deformation. Therefore, extrusion (as a finishing operation) provides high-strength properties of products due to strain hardening. Specifically, we shall present in this paper a numerical analysis of the extrusion of a case-shaped part together with the prediction of its damage by using the aforementioned two damage characteristics, ω_1 and ω_2.

In the next chapter we will, first, briefly state the axisymmetric MF-boundary value problem and, second, outline how it can be solved numerically and, in particular, how the two damage measures can be determined. This will then be followed by a results section including a discussion of the outcome of the analysis: Chapter 3. We would like to point out that the extensive experience of the two Russian authors in the method of characteristics of flow lines was used to achieve this task. Clearly, in principle, it would have been possible using other numerical techniques instead, e.g., the Finite Element Method (FEM), maybe even in context with commercial FE-codes and user-defined subroutines. However, this has not been done in order to demonstrate the feasibility of the approach in due course. Alternative analyses are left to future research. Moreover note that we will frequently refer to Part I of this paper [21] where further details of the underlying damage theory are explained.

2 The constitutive equations for damage analysis

Extrusion is a manufacturing process in which a blank of material, usually a metal, is pressed in a forming container by the mechanical action of a punch [18]. The container, whose shape is the inverse of the shape of the product, forces the solid material to yield in the backward direction of the pressing punch (*backward extrusion*). Extrusion results in high strength of the processed material as a consequence of strain hardening. Furthermore, a major advantage of the extrusion process is a highly compressive stress state, i.e., stress triaxiality $\langle\bar{\sigma}\rangle < -1$. Such a state of stress promotes a certain healing of the material, e.g., cracks and voids accumulated during MF may close, and, therefore, the obtainable degree of deformation is comparatively high [15]. Note that this is in contrast to other forming processes, such as deep drawing, where a sheet of metal is pressed into a forming die. In typical deep drawing processes stress triaxiality rises up to $\langle\bar{\sigma}\rangle \approx +2/3$ [2]. Consequently, at approximately 60% of straining the accumulated micro-defects result in macroscopic damage. In contrast to that the compressive regime of backward extrusion allows for straining up to 90% and more.

In the following, we will analyze the state of stress and the material properties of an axisymmetric case-shaped part made of a cylindrical Al-Mg bar (cf., Fig. 1, right). Specifically, two integral measures of strain damage, ω_1 and ω_2, connected with the second-rank tensor of damage ω_{ij}, will be used for the meso-structural parameters of the plastic material during the solution of the case study in this paper. The kinetic equation for the damage measure ω_1, which is related to plastic dilatation of the deformed material due to an increase in

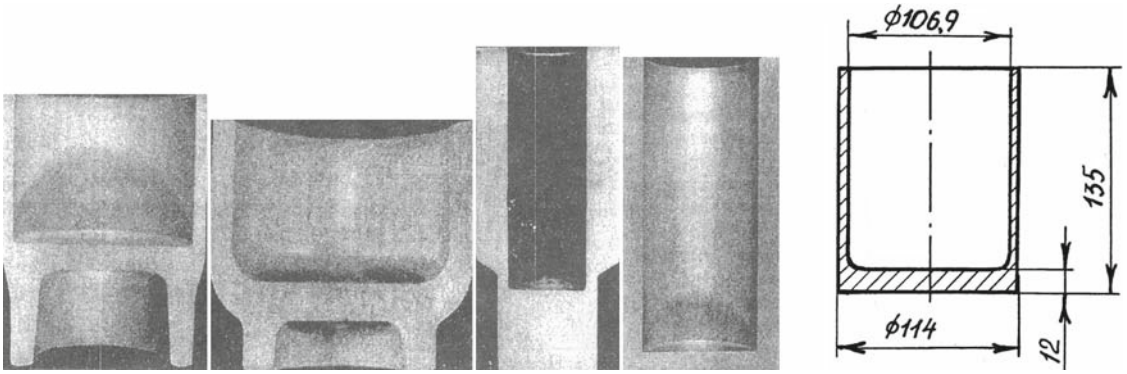

Fig. 1 Some typical axisymmetric case-shaped parts obtained by extrusion (*left*); draft for calculations (*right*)

micro-defect volume, is

$$\frac{\mathrm{d}\omega_1}{\mathrm{d}t} = \frac{1}{\varepsilon^{i}_{\cdot i}\,(\Lambda_{\lim})} \cdot \frac{\mathrm{d}\varepsilon^{i}_{\cdot i}\,(\Lambda)}{\mathrm{d}\Lambda} \cdot \frac{\mathrm{d}\Lambda}{\mathrm{d}t} \equiv \frac{\left[\varepsilon^{i}_{\cdot i}(\Lambda)\right]'\,\dot{\Lambda}}{\varepsilon^{i}_{\cdot i}(\Lambda_{\lim})}, \tag{1}$$

where $\varepsilon^{i}_{\cdot i}(\Lambda)$ is the empirically obtained dependence of plastic dilatation $\varepsilon^{i}_{\cdot i}$ (i.e., the first invariant of the plastic strain tensor ε_{ij}) on the cumulative strain at shear Λ, $\dot{\Lambda} = \mathrm{d}\Lambda/\mathrm{d}t$ is the shear strain rate, $\Lambda_{\lim}$ is the limit strain of the material at the moment of its macro-destruction, t denotes time, and the dash refers to differentiation with respect to Λ.

The cumulative shear strain, Λ, or Odquist parameter, is determined by

$$\Lambda = \int_{s(t)} \sqrt{2\dot{e}^{i}_{\cdot j}\dot{e}^{j}_{\cdot i}}\,\mathrm{d}t, \tag{2}$$

where $\dot{e}^{i}_{\cdot j}$ denote the mixed components of the deviatoric strain rates; $s(t)$ is a strain path [21].

The kinetic equation for the damage measure ω_2, which is connected with a change in micro-defect (void) shape under plastic deformation, takes on the following form:

$$\frac{\mathrm{d}\omega_2}{\mathrm{d}t} = \frac{\dot{\widehat{e}}}{\widehat{e}_{cr}} \equiv \frac{\sqrt{(1/2)\left(\dot{\widehat{e}}^{i\cdot}_{\cdot j}\,\dot{\widehat{e}}^{j\cdot}_{\cdot i}\right)}}{\widehat{e}_{cr}}, \tag{3}$$

where $\dot{\widehat{e}}$ is the equivalent deviatoric strain rate of voids, $\widehat{e}_{cr}$ is the critical deviatoric strain of voids corresponding to a stage of intense coalescence of ellipsoidal voids and formation of cavernous defects, and $\dot{\widehat{e}}^{i\cdot}_{\cdot j}$ are the mixed components of the deviatoric strain rate of voids.

The damage measures are defined over the following range: $\omega_1, \omega_2 \in [0; 1]$, where the upper-range value $\omega_1 = 1$ corresponds to the moment of macro-fracture, and $\omega_2 = 1$ corresponds to the stage of formation of cavernous defects (i.e., a stage of the micro-destruction at meso-scale). It should be noted that in [21] the authors related their own tensorial model of damage to commonly known models of void growth (e.g. [3,6,12,13]). The connection between the volume fraction of voids, f_v (considered as a measure of damage in a number of known models), the criterion of damage, ω (a dissipative damage theory, e.g., [6]), and the authors' measure of damage, ω_1 (a tensorial theory), is discussed there. Two classical approaches (criteria f_v and ω) were compared with a tensorial theory (i.e., in terms of the measures ω_1 and ω_2).

As outlined in detail in [21] the evolution of the yield stress σ_s can be described by

$$\sigma_s = \sigma_s^{(\mathrm{is})} \exp\left[-\alpha\left(\frac{T - T_0}{T_{\max} - T_0}\right)^{q}\right], \tag{4}$$

where $\sigma_s^{(\mathrm{is})} = \sigma_s^{(\mathrm{is})}(e_i, \dot{e}_{i0}, T_0, \mu_k)$ refers to isothermal hardening curves obtained for various materials at a fixed strain rate $\dot{e}_{i0}$ and an initial thermodynamic temperature T_0, e_i is an intensity of the cumulative strains,

Table 1 Parameters of plastically deformed Al-Mg alloy (temperature $T = 300-500$ K, strain rate $\dot{e}_i = 5-12\ \mathrm{s}^{-1}$)

σ_0, MPa	$\sigma_{d\|\omega=0}$, MPa	A, MPa	m	$l \cdot 10^{-2}$, mm	B, MPa	n_0	n_1	T_0, K	$T_{\max}$, K	α	q
140	211	186	1.161	0.774	273	0.439	0.267	300	800	1.380	1.000

Table 2 Material parameters for calculations of damage and internal energy of hardening

Parameters of plastic dilatation		Parameters of limit plasticity			Damage of the as-delivered material	
b	a	A	B	c	ω_{10}	ω_{20}
0.150	1.280	−0.033	2.833	0.569	0–0.08	0–0.10

μ_k are meso-structural parameters, T and $T_{\max}$ are the current and the maximum temperature of the process, respectively, α and q are parameters used in the equation for the temperature dependent yield strength σ_s [21]. The isothermal yield stress can be written as follows:

$$\sigma_s^{(\mathrm{is})} = \sigma_0 + \left(\sigma_{d/\omega=0} + A\omega^m\right)\ D^{-\frac{1}{2}} l^{\frac{1}{2}} + B e_i^{(n_0 - n_1 e_i)}, \tag{5}$$

where σ_0 is the initial yield stress given by the resistance to the movement of free dislocations, ω is the strain damage related to plastic dilatation induced by micro-defect growth, and σ_d is a stress required for the movement of locked dislocations which will be specified below. Moreover, A and m are parameters of the relationship $\sigma_d = \sigma_d(\omega)$, D is average grain size, l is a characteristic distance from the grain boundary to the nearest dislocation source, and B, n_0, and n_1 are scalar parameters describing the work hardening of the yield stress in an isothermal regime.

The material of the as-delivered primary blanks is an Al-Mg alloy (after recrystallization annealing) with material parameters summarized in Table 1. During the extrusion we assume a constant processing speed with strain rates of $\dot{e}_i = 5$–$12\ \mathrm{s}^{-1}$ and a given temperature of $T = 300$–500 K. Note that this temperature is still below the recrystallization temperature of the Al-Mg alloy.

Substituting the data of Table 1 with Eqs. (4) and (5) we may determine the yield stress of Al-Mg alloy to depend on strain hardening and micro-structural changes by

$$\sigma_s = \sigma_s^{(\mathrm{is})} \exp\left(-1.38\frac{T-300}{500}\right), \sigma_s^{(\mathrm{is})} = 140 + 0.774 \cdot 10^{-2}(211 + 186\omega^{1.161})\ D^{-\frac{1}{2}} + 273 e_i^{(0.439 - 0.267 e_i)}. \tag{6}$$

The strain damage of the finished part can be predicted by numerical integration of Eqs. (1) and (3) for the damage parameters ω_1 and ω_2. The function of plastic dilatation, $\varepsilon_{\cdot i}^{i}(\Lambda)$, that appears in Eq. (1), is of the power type, $\varepsilon_{\cdot i}^{i}(\Lambda) = b\Lambda^a$, where b and a denote experimentally determined parameters (cf., Table 2). Therefore Eq. (1) becomes

$$\mathrm{d}\omega_1 = \frac{a\Lambda^{a-1}}{\Lambda_{\lim}^a}\mathrm{d}\Lambda. \tag{7}$$

The limit cumulative strain at shear, $\Lambda_{\lim}$, appearing in Eq. (7), corresponds to the destruction of the deformed material. The limit strain $\Lambda_{\lim}$ is determined by experimental diagrams of plasticity plotted for the investigated Al-Mg alloy under prescribed temperature-speed conditions (cf., Fig. 11 in [21]). Plasticity diagrams represent the experimentally determined dependence of the limit strain $\Lambda_{\lim}$ on stress triaxiality $\langle\bar{\sigma}\rangle$, which can be approximated by a power function in the following form:

$$\Lambda_{\lim} = A \cdot \exp\left(-\langle\bar{\sigma}\rangle\right) + B \cdot \exp\left(-c\,\langle\bar{\sigma}\rangle\right), \tag{8}$$

where A, B, c are the experimentally determined parameters (cf., Table 2).

Proceeding in Eq. (7) with small finite increments of the strain ($\Delta\Lambda$) we may find the material damage after the kth stage of deformation by numerical integration:

$$\omega_{1k} = \omega_{10} + \sum_{j=1}^{k}\Delta\omega_{1j}, \quad \Delta\omega_{1j} = \frac{a\Lambda_j^{a-1}}{\Lambda_{\lim}^a\left(\langle\bar{\sigma}\rangle_j\right)}\Delta\Lambda_j, \tag{9}$$

where ω_{10} is the damage of the as-delivered material (cf., Table 2), Λ_j is the strain accumulated by the material particles up to the jth stage, $\Lambda_{\lim}(\langle\bar{\sigma}\rangle_j)$ is the limit strain corresponding to stress triaxiality $\langle\bar{\sigma}\rangle_j$ at the jth stage.

Calculations of the damage measure ω_2 by means of numerical integration of the kinetic equation (3) are connected with the determination of the equivalent deviatoric strain rate of voids $\dot{\widehat{e}}$, and the critical deviatoric strain $\widehat{e}_{cr}$ corresponding to a stage of intense coalescence of ellipsoidal voids and formation of cavernous defects. Calculations of the equivalent strain rate of voids necessitate an experimental determination of their dimensions changing under deformation [11,19]. The determination of the critical equivalent strain $\widehat{e}_{cr}$ of voids in the investigated materials is based on microscopic analysis of void coalescence in test specimens during their stage-by-stage plastic deformation. The obtained micrographs will allow us to detect a stage of intense void coalescence into large cavernous defects. Such experiments involve great technical difficulties [10]. This is why we shall make use of statistical characteristics of void formation.

For instance, the averaged equivalent strain rate can be applied within each Representative Volume Element (RVE). A corresponding measure is the equivalent strain rate ($\dot{\boldsymbol{e}}$) of the RVE. The hypothesis that it is possible to model the void deformation by using the strain measures of the RVE requires detailed experimental verification. The experimental justification of this hypothesis will allow us to predict shape changes and coalescence of voids by means of accompanying axes ξ^i plotted as coordinate grids on deformed specimens and manufacturing blanks. This hypothesis allows us to accept in our case $\dot{\widehat{e}}(r,z,t) = \dot{\boldsymbol{e}}(r,z,t)$, where the function $\dot{\boldsymbol{e}}(r,z,t)$ can be established by a distribution of the equivalent strain increments $\Delta\boldsymbol{e}(r,z,h)$ in cells of the coordinate grid, i.e., $\dot{\boldsymbol{e}}(r,z,t) \cong \Delta\boldsymbol{e}(r,z,t)/\Delta t = \upsilon_{\mathrm{p}} \cdot \Delta\boldsymbol{e}(r,z,h)/\Delta h$.

In order to find the critical equivalent strain of voids, $\widehat{e}_{cr}$, the experimental results obtained by Bogatov et al. [1] were used. They investigated void coalescence and formation of cavernous defects in some structural metals at forming. Electron-probe analysis of the micro-structure of stepwise deformed metals allowed them to verify that the critical equivalent strain of voids can be expressed as $\widehat{\boldsymbol{e}}_{cr} = 0.6 \cdot \boldsymbol{e}_{\lim} \exp[0.05(1 - \langle\bar{\sigma}\rangle)]$, where $\boldsymbol{e}_{\lim} = \Lambda_{\lim}/2$ is the limit deviatoric strain of RVE corresponding to the moment of its destruction. In view of the given experimental data Eq. (3) becomes

$$\mathrm{d}\omega_2 = \frac{5 \cdot \exp\left[0.05\left(\langle\bar{\sigma}\rangle - 1\right)\right]}{3 \cdot \boldsymbol{e}_{\lim}} \mathrm{d}\boldsymbol{e}. \tag{10}$$

By using small finite strain increments, $\Delta\boldsymbol{e}$, in Eq. (10) we may calculate the material damage ω_2 after the kth stage of deformation by numerical integration

$$\omega_{2k} = \omega_{20} + \sum_{j=1}^{k} \Delta\omega_{2j}, \quad \Delta\omega_{2j} = \frac{5 \cdot \exp\left[0.05\left(\langle\bar{\sigma}\rangle_j - 1\right)\right]}{3 \cdot \boldsymbol{e}_{\lim\, j}} \left(\Delta\boldsymbol{e}\right)_j, \tag{11}$$

where ω_{20} is the damage of the as-delivered material (cf., Table 2), and $\boldsymbol{e}_{\lim\, j}$ is the limit deviatoric strain corresponding to the stress state parameter $\langle\bar{\sigma}\rangle_j$ at the jth stage of deformation.

The cumulative strain Λ (including the equivalent strain $\boldsymbol{e} = \Lambda/\sqrt{3}$) and stress triaxiality $\langle\bar{\sigma}\rangle$ appears in the constitutive equations for damage measures (1), (7), (8), (10). In turn, the cumulative strain Λ and stress triaxiality $\langle\bar{\sigma}\rangle$ can be determined in each nodal point of the deformed material by using mutually consistent fields of stresses, σ_{ij}, and plastic flow velocities, υ_i. Hence, damage analysis in processes with plastic flow of metals is a coupled problem of the calculation of stresses, flow velocities, and strains as well as mechanical and meso-structural characteristics of the deformed material.

To calculate the stress-strain state we use the equations describing axisymmetric plastic flow of metals in *Eulerian* cylindrical coordinates, where r, z, θ denote the radial, the axial, and the circumferential direction, respectively. The basic equations of plasticity are given by the differential equations of equilibrium

$$\frac{\partial\sigma_r}{\partial r} + \frac{\partial\tau_{rz}}{\partial z} + \frac{\sigma_r - \sigma_\theta}{r} = 0\,, \quad \frac{\partial\tau_{rz}}{\partial r} + \frac{\partial\sigma_z}{\partial z} + \frac{\tau_{rz}}{r} = 0, \tag{12}$$

the von Mises yield surface

$$(\sigma_r - \sigma_z)^2 + (\sigma_z - \sigma_\theta)^2 + (\sigma_\theta - \sigma_r)^2 + 6\tau_{rz}^2 = 6\tau_s^2, \tag{13}$$

the condition of coaxiality of the strain rate deviator, $\dot{e}_{ij}$, and the stress deviator, s_{ij}:

$$\frac{\partial \upsilon_r/\partial z + \partial \upsilon_z/\partial r}{2\tau_{rz}} = \frac{\partial \upsilon_r/\partial z - \partial \upsilon_z/\partial r}{\sigma_r - \sigma_z}, \tag{14}$$

the condition of similarity of the deviators $\dot{e}_{ij}$ and s_{ij} (15), i.e., of coincidence of their Lode angles, $\phi_{\dot{e}}$ and ϕ_σ [21]

$$\sqrt{\frac{I_2(\dot{e}_{ij})}{I_2(s_{ij})}} = \sqrt[3]{\frac{I_3(\dot{e}_{ij})}{I_3(s_{ij})}}, \tag{15}$$

and the incompressibility condition

$$\frac{\partial \upsilon_r}{\partial r} + \frac{\partial \upsilon_z}{\partial z} + \frac{\upsilon_r}{r} = 0, \tag{16}$$

where $\sigma_r, \sigma_z, \sigma_\theta, \tau_{rz}$ are nonzero components of the stress tensor σ_{ij}, τ_s is the yield stress for shear, υ_r, υ_z are the components of the vector of plastic flow velocity, $I_2(\dot{e}_{ij}) = \dot{\boldsymbol{e}}^2$, $I_3(\dot{e}_{ij})$, $I_2(s_{ij}) = \boldsymbol{s}^2$, $I_3(s_{ij})$ are the second and the third invariants of deviatoric strain rates $\dot{e}_{ij}$ and deviatoric stresses s_{ij}, respectively, and $\dot{\boldsymbol{e}}$, $\boldsymbol{s}$ denote the equivalent deviatoric strain rate and stress.

The deformed material is considered as a rigidly-plastic solid because plastic strains amount to 70–90% at MF being $\approx 10^2$ larger than elastic strains [21]. The axisymmetric stress-strain state has the following features: for the stress components we have $\tau_{z\theta} = \tau_{\theta r} = 0$, $\upsilon_\theta = 0$. The hoop stress σ_θ is a principal stress. In order to represent the axisymmetric stress-strain state completely it will be sufficient to determine a field of stresses and flow velocities in one of the meridian cross-sections of the deformed solid.

For the analysis of MF processes with a rapidly changing stress state the basic differential equations for axisymmetric plastic flow are solved by hyperbolic approximations [16]. The technique is based on a representation of yield zones in a special form for the stresses related to Iljushin's deviatoric stress space [5]. Actually, this technique represents the enhanced slip line method for solving the problems of axisymmetric plastic flow with the intense change of stress state. The information on slip line fields (i.e., directions of microscopic shear bands) in plastic zone of the deformed material proves to be very useful when modeling the nucleation of voids. It is experimentally known that large voids generate microscopic shear bands. Voids nucleate, grow, and coalesce within these shear bands, finally forming large cavities (20–30 μm) [20].

The slip lines form two families of mutually orthogonal lines (α and β) in the meridian cross-section of the plastic zone

$$\frac{\mathrm{d}z}{\mathrm{d}r} = \tan\delta_\theta \text{ (at line } \alpha), \quad \frac{\mathrm{d}z}{\mathrm{d}r} = -\tan\delta_\theta \text{ (at line } \beta), \tag{17}$$

where δ_θ is the angle between the r-axis and the line α. The angle δ_θ is connected with the stress components by the following relation:

$$\tan 2\delta_\theta = -\frac{\sigma_r - \sigma_z}{2\tau_{rz}}, \tag{18}$$

which can be used in the basic solution as the additional condition in terms of stresses.

When solving the basic equations (12)–(16) it is convenient to use a special representing space of the parameters $\varphi_\theta, m_\theta, m_r, m_z$ which are introduced by the following relations:

$$\begin{gathered} \mathrm{tg}2\varphi_\theta = \sqrt{\tfrac{2}{3}\tan 2\delta_\theta}, \ \boldsymbol{s}m_\theta \cos 2\varphi_\theta = \tau_{\alpha\beta}\cos 2\delta_\theta \\ I_1\left(\bar{s}_{ij}\right) = m_\theta \sin 2\varphi_\theta - m_r \mathrm{sign}\,(\sigma_z - \sigma_\theta) - m_z \mathrm{sign}\,(\sigma_\theta - \sigma_r) = 0, \ I_2(\bar{s}_{ij}) = m_\theta^2 + m_r^2 + m_z^2 = 1 \end{gathered} \tag{19}$$

where $I_1(\bar{s}_{ij}) = 0$, $I_2(\bar{s}_{ij}) = 1$ are the first and the second invariants of the directing stress deviator $\bar{s}_{ij} = s_{ij}/\sqrt{I_2(s_{ij})} \equiv s_{ij}/\boldsymbol{s}$, and $\mathrm{sign}(\sigma_z - \sigma_\theta)$, $\mathrm{sign}(\sigma_\theta - \sigma_r)$ are the sign functions, *i.e.*, the signs of the arguments $(\sigma_z - \sigma_\theta)$ and $(\sigma_\theta - \sigma_r)$.

The representing space of the parameters $\varphi_\theta, m_\theta, m_r, m_z$ is connected with Iljushin's deviatoric space [5]. The sign functions $\mathrm{sign}(\sigma_z - \sigma_\theta)$ and $\mathrm{sign}(\sigma_\theta - \sigma_r)$ that appear in Eqs. (19) depend on the type of processing operations. In processes with predominant axial compression (e.g., extrusion, upsetting, bulk forging) we have

$$\sigma_r \geq \sigma_\theta \geq \sigma_z, \quad \mathrm{sign}\,(\sigma_z - \sigma_\theta) = -1, \quad \mathrm{sign}\,(\sigma_\theta - \sigma_r) = -1.$$

Physically speaking, the parameters m_θ, m_r, m_z define a direction of the vector of the octahedral shear stress, τ_8, which is within the deviatoric plane $(19)_3$ [7]. Eqs. (12) in combination with the parametric representation of stresses (19) takes the following form in the system of coordinates α and β:

$$\begin{aligned}
&\frac{\partial\langle\sigma\rangle}{\partial s_\alpha} - 2\tau_s m_\theta\left[1+\sqrt{\frac{2}{3}}\varphi'(\delta_\theta)\right]\frac{\partial\delta_\theta}{\partial s_\alpha} - \frac{\sqrt{1-m_\theta^2}}{\sqrt{3}}\operatorname{sign}(\sigma_\theta-\sigma_\alpha)\frac{\partial\tau_s}{\partial s_\alpha} + m_\theta\frac{\partial\tau_s}{\partial s_\beta}\\
&\quad+\tau_s\frac{m_\theta}{\sqrt{3}\sqrt{1-m_\theta^2}}\operatorname{sign}(\sigma_\theta-\sigma_\alpha)\frac{\partial m_\theta}{\partial s_\alpha} + \tau_s\frac{\partial m_\theta}{\partial s_\beta} - \sqrt{3}\frac{\tau_s}{r}\sqrt{1-m_\theta^2}\cos\delta_\theta\operatorname{sign}(\sigma_\theta-\sigma_\alpha)\\
&\quad-\tau_s\frac{m_\theta}{r}\sin\delta_\theta = 0, \qquad (20)\\
&\frac{\partial\langle\sigma\rangle}{\partial s_\beta} + 2\tau_s m_\theta\left[1+\sqrt{\frac{2}{3}}\varphi'(\delta_\theta)\right]\frac{\partial\delta_\theta}{\partial s_\beta} + m_\theta\frac{\partial\tau_s}{\partial s_\alpha} - \frac{\sqrt{1-m_\theta^2}}{\sqrt{3}}\operatorname{sign}(\sigma_\theta-\sigma_\alpha)\frac{\partial\tau_s}{\partial s_\beta}\\
&\quad+\sqrt{3}\frac{\tau_s}{r}\sqrt{1-m_\theta^2}\sin\delta_\theta\operatorname{sign}(\sigma_\theta-\sigma_\alpha) + \tau_s\frac{\partial m_\theta}{\partial s_\alpha} + \tau_s\frac{m_\theta}{\sqrt{3}\sqrt{1-m_\theta^2}}\operatorname{sign}(\sigma_\theta-\sigma_\alpha)\frac{\partial m_\theta}{\partial s_\beta}\\
&\quad+\tau_s\frac{m_\theta}{r}\cos\delta_\theta = 0, \qquad (21)
\end{aligned}$$

where $\langle\sigma\rangle$ indicates hydrostatic stress and $\varphi'_\theta(\delta_\theta) = \mathrm{d}\varphi'_\theta/\mathrm{d}\delta_\theta$, $m_\alpha = m_\beta = \frac{1}{\sqrt{2}}\sqrt{1-m_\theta^2}$.

Equations (14) and (16) for the velocities can be rewritten in terms of fixed coordinates α^* and β^* coinciding with trajectories α and β:

$$\frac{\partial\upsilon_{\alpha^*}}{\partial s_\alpha} - \upsilon_{\beta^*}\frac{\partial\delta_\theta}{\partial s_\alpha} + \frac{\upsilon_{\alpha^*}\cos\delta_\theta - \upsilon_{\beta^*}\sin\delta_\theta}{r} = 0, \qquad (22)$$

$$\frac{\partial\upsilon_{\beta^*}}{\partial s_\beta} - \upsilon_{\alpha^*}\frac{\partial\delta_\theta}{\partial s_\beta} + \frac{\upsilon_{\alpha^*}\cos\delta_\theta - \upsilon_{\beta^*}\sin\delta_\theta}{2r} = 0. \qquad (23)$$

The solution of Eqs. (15), (20)–(23) satisfy Cauchy-type boundary conditions. In case of an axisymmetric problem the Cauchy-type conditions are given by boundary values of the required functions $\langle\sigma\rangle$, δ_θ, m_θ, υ_{α^*}, υ_{β^*} at the two-dimensional surface $\omega(\alpha^*, \beta^*) = 0$ in the space α^*, β^*.

The four partial differential equations (20)–(23) are closed w.r.t. five required functions $\langle\sigma\rangle$, δ_θ, m_θ, υ_{α^*} and υ_{β^*} by means of the differential constraint (15). These four equations are of hyperbolic type and have two pair-wise coincident sets of mutually orthogonal characteristics, α and β. The characteristic lines α and β coincide with the slip lines and they are described by Eq. (17). This allows us to use grid-characteristic schemes for the numerical solution of arising boundary problems.

3 Results and discussion

Since the characteristics of damage depend on strain history a stepwise analysis of the forming process together with a detailed determination of stress-strain state is necessary for their calculation. For the purpose of the analysis the process of extrusion will be divided into three stages. The first stage is characterized by contraction of the blank with the initial height, $h_0 = 33.1$ mm, and filling of the space between the container and the blank. It ends with outflow into the clearance. During this stage the height of the blank slightly decreases with a typical degree of deformation of $\varepsilon_\mathrm{I} = 0.01 - 0.02$. Here we put $\varepsilon_\mathrm{I} = 0.018$ and thus we obtain for the difference of initial and final height in the first stage, $\Delta h_1 = \varepsilon_\mathrm{I}\cdot h_0 = \Delta h_1 = 0.60$ mm. The second stage is characterized by a constant shape and size of the plastic zone. Plastic flow at this stage is stationary with a decreasing height of the blank and an outflow into the clearance between the container and the punch. In the third stage the plastic zone spreads over all the material under the punch. The plastic flow is now non-stationary.

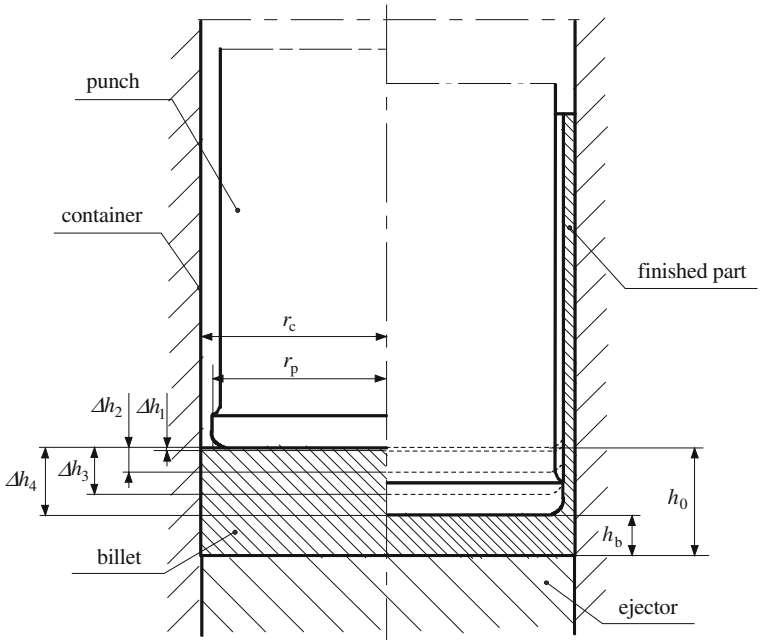

Fig. 2 Extrusion of a case-shaped part (Δh_i denotes a displacement of the punch at a moment i, where $i = 1 \cdots 4$)

The stress-strain state is evaluated at four stages (cf., Fig. 2), as follows:

1. at the initial moment of the second stage when $\Delta h_1 = 0.60$ mm,
2. at an intermediate moment when $\Delta h_2 = 7.45$ mm,
3. at an intermediate moment when $\Delta h_3 = 14.30$ mm,
4. at the final state, i.e., $\Delta h_4 = 21.10$ mm.

By solving the boundary problem we may construct a field of slip lines (i.e., characteristics) in the meridian cross-section of the axisymmetrically deformed material. Then the contour of the plastic zone is determined, and stress components are calculated (cf., Fig. 3).

Note, that the defining differential equations (2) and (20)–(23) are represented in recursive form for numerical calculations [17]. When solving these boundary value problems we use a condition of maximum contact friction at the end surface of the punch and at the back surface of the container, i.e., $\tau_c = \tau_{\alpha\beta}$ (τ_c denotes the shearing stress at the contact). The normal pressure of the deformed metal on a lateral surface of the container is much lower than on its back surface. Therefore, a condition of the Prandtl-type for non-maximum contact friction is realized at a lateral surface of the container

$$\tau_c = f_p \tau_{\alpha\beta} = f_p m_\theta \tau_s, \tag{24}$$

where $f_p \in [0; 1]$ is a coefficient of plastic friction.

Then the flow velocity fields are determined at the observed moments of extrusion, (cf., Fig. 4). The known field of slip lines (α, β) allows us to use the velocity equations (22) and (23) when determining the velocities υ_{α^*}, υ_{β^*} in the nodal points, since the angle δ_θ and the coordinate arcs s_α, s_β are already known from the solution for the stress components. The velocity fields in Fig. 4 are determined by solving the boundary problems. A grid of lines $\bar{\alpha}$, $\bar{\beta}$ selected in the plastic zone consists of continuum points. This grid is coincident with a grid of the trajectories (or characteristics) α, β at the observed moment of deformation. This grid of the material lines $\bar{\alpha}$, $\bar{\beta}$ can be considered as an associated coordinate frame [14], and the constructed velocity field (*cf.*, Fig. 4a) can be considered as a representation of the material lines $\bar{\alpha}$, $\bar{\beta}$ in the velocity plane. A similar representation of the flow velocity field is essential when modeling the non-stationary processes of plastic deformation. The kinematic relations (20) and (21) can be applied to the continuum lines $\bar{\alpha}$, $\bar{\beta}$ which are coincident with the slip lines α, β. During non-stationary flow a grid of the slip lines α, β [characteristics of Eqs. (20)–(23)] is displaced w.r.t. the material lines $\bar{\alpha}$, $\bar{\beta}$.

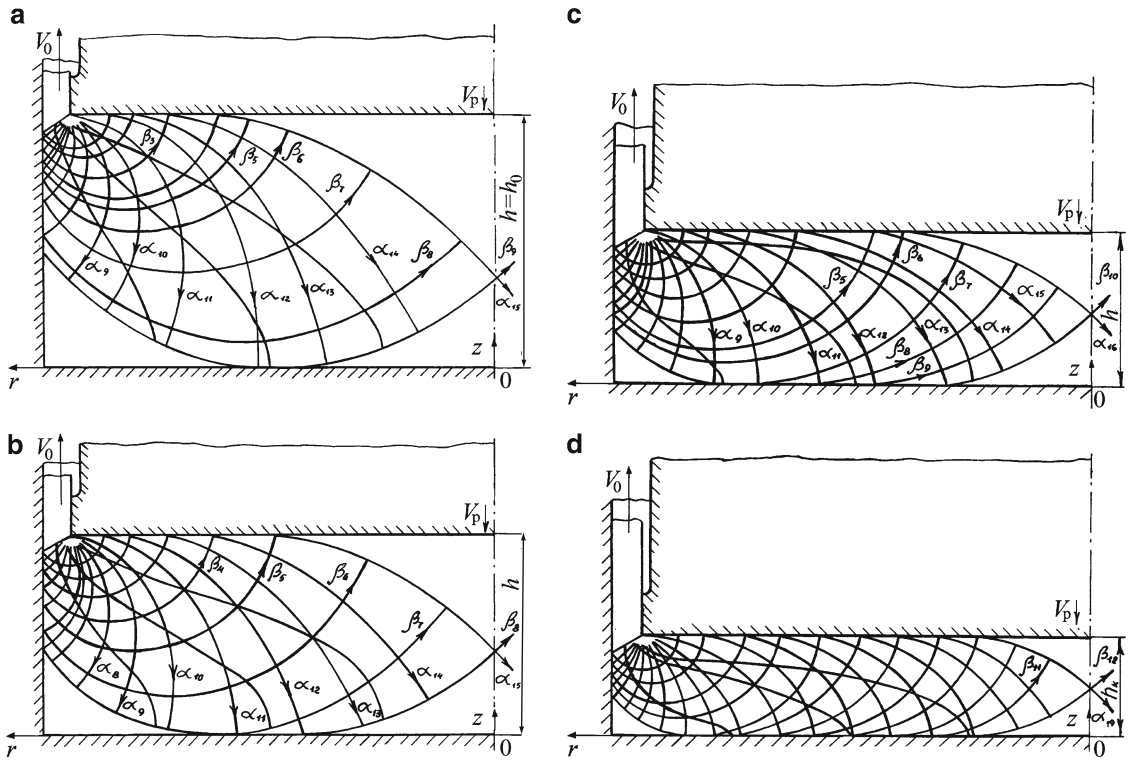

Fig. 3 Extrusion of the axisymmetric case-shaped part (final non-stationary stage): the plastic zone, stress field, flow lines for various punch displacements: **a** $\Delta h_1 = 0.60$ mm; **b** $\Delta h_2 = 7.45$ mm; **c** $\Delta h_3 = 14.30$ mm; **d** $\Delta h_4 = 21.10$ mm

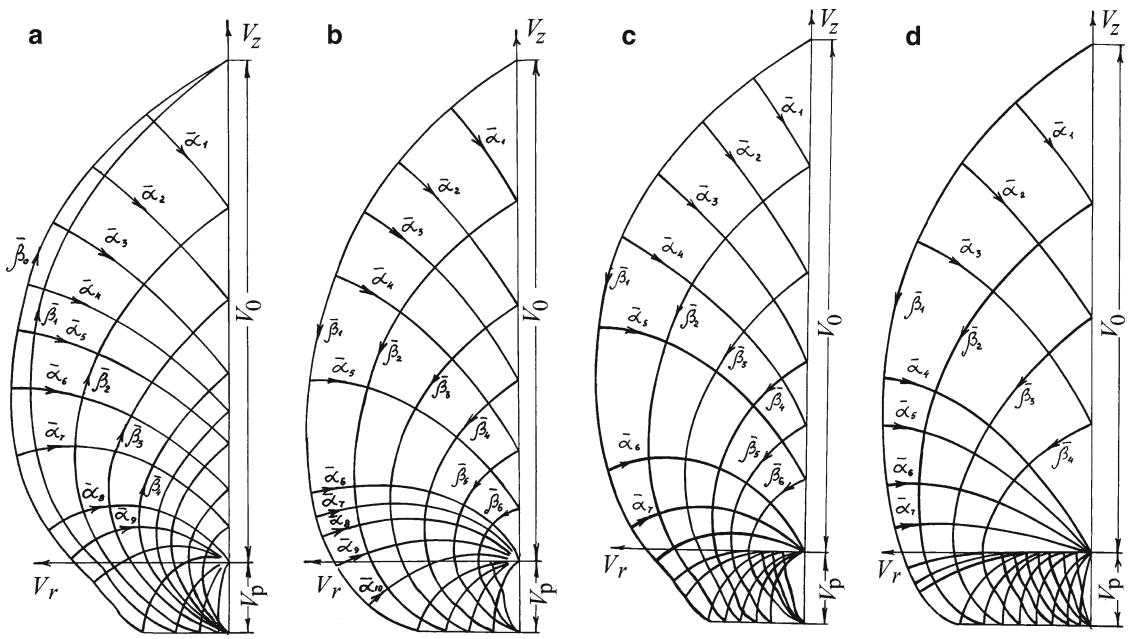

Fig. 4 The velocity field during extrusion of the axisymmetric case-shaped part (the final non-stationary stage) for various punch displacements: **a** $\Delta h_1 = 0.60$ mm; **b** $\Delta h_2 = 7.45$ mm; **c** $\Delta h_3 = 14.30$ mm; **d** $\Delta h_4 = 21.10$ mm

The velocity field has the following typical feature for an axisymmetric process: The angle between the lines $\bar{\alpha}$ and $\bar{\beta}$ increasingly changes from $\pi/2$ to π, when we map the lines $\bar{\alpha}$, $\bar{\beta}$, which are close to the symmetry axis of the blank, onto the plane of velocities υ_r, υ_z. Thus the representation of the material lines $\bar{\alpha}$ and $\bar{\beta}$ in the plane of velocities υ_r, υ_z depends on the Lode angle.

The degree of conformity between the fields of stresses $\sigma_{ij}^{(0)}$ and velocities $\upsilon_i^{(0)}$ in the basic solution is determined by fulfilling the similarity condition (15) for the deviators $\dot{e}_{ij}$ and s_{ij} in the form

$$m_\theta^{(\dot{e})} - m_\theta^{(\sigma)} \le [\Delta m_\theta]\,, \tag{25}$$

$[\Delta m_\theta]$ being a permissible mismatch error for the parameters $m_\theta^{(\dot{e})}$ and $m_\theta^{(\sigma)}$ related to the fields of stresses and strain rates.

For the solution of the inequality (25) the method of group relaxation is used (e.g., [9, Section 20.3–2]). By regulating the absolute value of the difference between the parameters $m_\theta^{(\dot{e})}$ and $m_\theta^{(\sigma)}$ in selected nodes of the plastic zone (instead of bringing it down to be zero in the first step) it is possible to fulfill the inequality (25) already at the first correction with the permissible error $[\Delta m_\theta] = 0.01$. The calculated stress field (cf., Fig. 3) and the corresponding field of flow velocities (cf., Fig. 4) satisfy the inequality (25) for the permissible error $[\Delta m_\theta] = 0.01$.

The fields of stresses (σ_{ij}) and the plastic flow velocities (υ_i) found at the different stages of non-stationary deformation allow us to calculate cumulative strains (Λ). Cumulative strains Λ appear in the kinetic equations for meso-structural parameters (μ_k) of the deformed material, including the damage parameters ω_1 and ω_2. Cumulative strains are calculated along trajectories of movement of the material particles. The cumulative strains after stage k are $\Lambda_k = \sum_{j=1}^{k} \Delta\Lambda_j$, and $\Lambda = \sum_{j=1}^{n} \Delta\Lambda_j$ at the end of forming. In Fig. 6 the distribution of the cumulative strains Λ is shown for the radially directed middle layer of bottom part of the finished product ($z = 0.5h_\mathrm{b}$, where h_b is bottom thickness).

In order to verify the calculated strain distribution the strains are experimentally determined by means of a coordinate grid. This technique allows us to find fields of the shear strains $\Lambda(r, z)$ at different stages of extrusion. The fields $\Lambda(r, z)$ are used when determining the yield stress $\sigma_s^{(\mathrm{is})}(r, z)$ from the intensity of the cumulative strains $e_i(r, z) = \Lambda(r, z)/\sqrt{3}$, cf., Eq. (5), and, moreover, for finding the yield stress under shear $\tau_{sm.n}(r_{m.n}, z_{m.n}) = \sigma_s(r_{m.n}, z_{m.n})/\sqrt{3}$. The specimen is cut through its meridian cross-section in order to plot a coordinate grid (cf., Fig. 5). In Fig. 6 (*left*) the experimentally found distribution of the cumulative strains Λ is shown for the radially directed middle layer of bottom part of the finished product ($z = 0.5h_\mathrm{b}$). The calculated distribution of Λ satisfactorily fits the experimental results.

Now we have the complete information which is required to calculate damage measures using Eqs. (9) and (11). Moreover, we know the mechanical and meso-structural parameters of the Al-alloy (cf., Tables 1 and 2) as well as stepwise values of the strain, $\Delta\Lambda_i$, and the limit strain Λ_lim (as the known function of stress triaxiality $\langle\bar{\sigma}\rangle$, cf., (8)).

In Fig. 6 the predicted distribution of damage (ω_1 and ω_2) is shown for the radially directed middle layer of bottom of the finished product (with the coordinate $z = 0.5h_\mathrm{b}$). The obvious fact that the damage increases from the symmetry axis towards the walls can be explained as follows. First, the strain (Λ) accumulated by the material particles along their motion trajectories directed towards the walls increases in the same direction. Second, large compressive hydrostatic stress $\langle\sigma\rangle$ prevents the evolution of damage, and indeed, the absolute value of $\langle\sigma\rangle$ increases when moving from the walls toward the axis of symmetry.

Also note in Fig. 6 that the growth rate of ω_2 is higher than that of ω_1. The ratio of the increments $\mathrm{d}\omega_2/\mathrm{d}\omega_1 > 1$ follows from Eqs. (7) and (10). For example, $\mathrm{d}\omega_2/\mathrm{d}\omega_1 = 1.3 - 1.6$ when the triaxiality is $\langle\bar{\sigma}\rangle = -3 - 0.67$, which is typical for MF processes. In other words, this ratio is greater for tensile regimes of the stress state ($\langle\bar{\sigma}\rangle > 0$) than for compressive ones ($\langle\bar{\sigma}\rangle < 0$). These relations are physically obvious. Void coalescence always advances macro-crack formation. And during tensile loading regimes (when tensile stresses promote void growth) this advance will be greater than during compressive ones.

The predicted values of damage induced by micro-defects are much smaller than the allowed ones: $\omega_{1\max} = 0.42 < \omega_{1\mathrm{lim}} = 1$, $\omega_{2\max} = 0.51 < \omega_{2\mathrm{lim}} = 1$. High hydrostatic pressure in the plastic zone heals micro-defects prevents their growth and thereby enhances the processing ductility of the deformed metal. Thus, larger processing strains are possible during extrusion (up to 90% and more) when compared to deep-drawing (no more than 70–75%) when producing axisymmetric case-shaped parts.

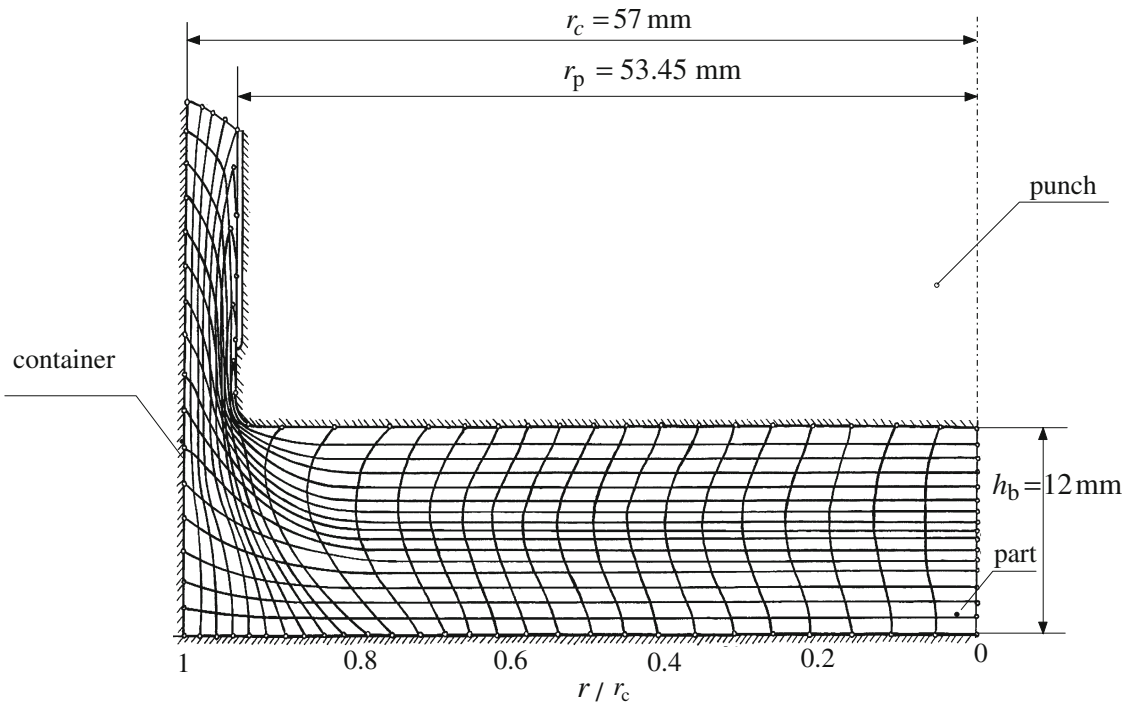

Fig. 5 Coordinate grid in a meridian cross-section of the case-shaped Al-Mg part at the final stage of extrusion

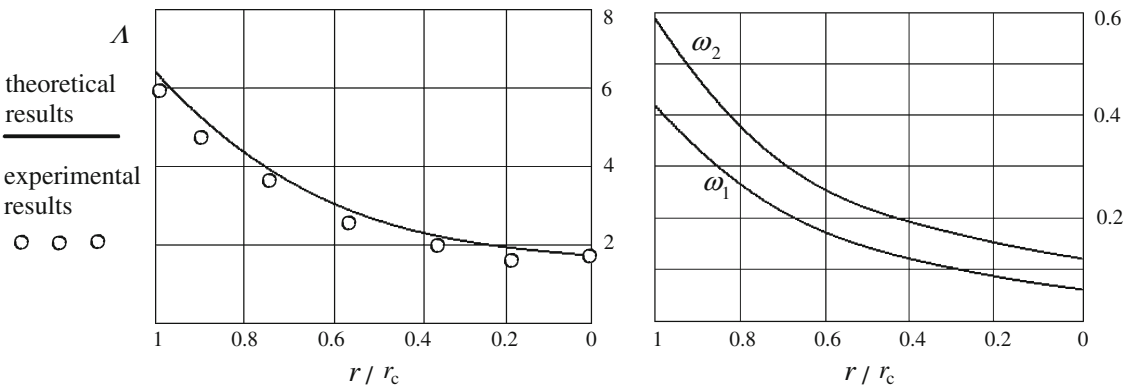

Fig. 6 Distribution of the strain Λ (*left*) and the damage measures ω_1, ω_2 (*right*) in the median layer ($z = 0.5h_b = 6$mm) of the meridian cross-section of the axisymmetric case-shaped Al-Mg part (with the outer radius $r_c = 57$ mm) after extrusion

4 Conclusions and outlook

In this section we will discuss some results of the analysis of extrusion of the axisymmetric case-shaped part. The type of the state of stress strongly varies within the volume of the processed metal from monoaxial compression at its symmetry axis to simple shear around the clearance between the punch and the container. This fact indicates complex loading of the deformed material, *i.e.*, a rotation of the principal axes of the stress tensor w.r.t. the deforming material lines and a change of proportions between the components of the stress tensor. Conditions of complex loading necessitate using the associated rule of plastic flow for the basic equations.

Cumulative strains are irregularly distributed in the bottom part of the finished product. The largest strain is accumulated by the material particles which appear out of the plastic zone or approach to its neighborhood at the final moment of processing. The reliability of the predicted mechanical and mesostructural characteristics depends on the accuracy of the calculated strain field. The strains that were experimentally determined from a coordinate grid satisfactorily agree with the theoretically calculated strains.

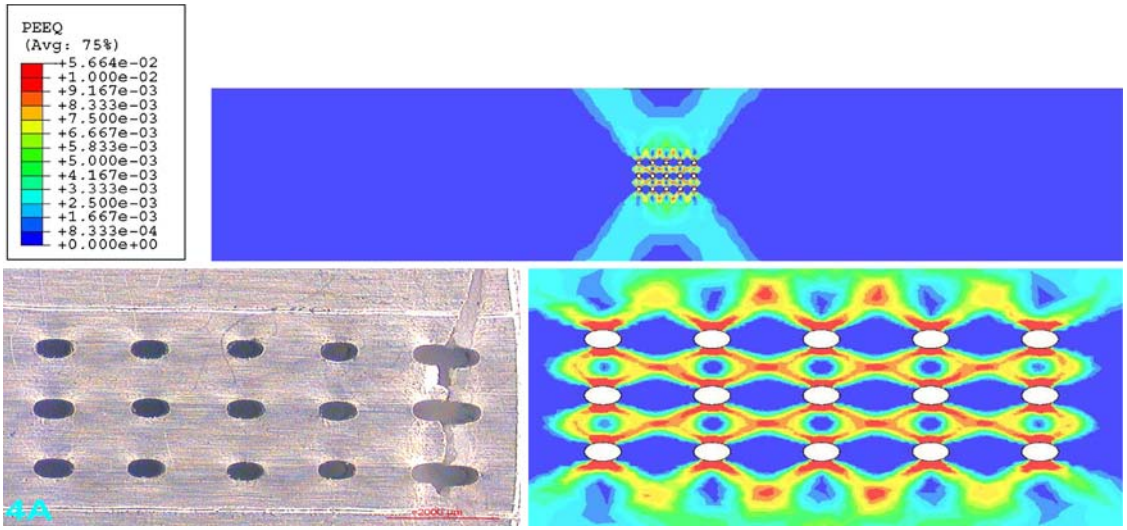

Fig. 7 *Top* plastic deformation of the sheet Al specimen subjected to uniaxial tension (FE simulation); *bottom* the plastic strain of the zone with imitation defects (*left* micrograph, *right* FE simulation)

Comparison between the maximum values of damage measures and their allowed values, *i.e.* $\omega_{1\max} = 0.42 < \omega_{1\lim} = 1, \omega_{2\max} = 0.51 < \omega_{2\lim} = 1$, allow us to predict the quality of the material structure after extrusion. Large processing strain at extrusion provides high-strength properties of products due to strain hardening.

The combined use of two damage measures, ω_1 and ω_2, in contrast to using only ω_1 or the volume fraction of voids, f_v, as in the known common models (cf., e.g., [3,6,12,13]), allows us to predict not only a risk of macro-fracture of the deformed material but even the stage of formation of large cavernous defects due to coalescence of voids taking a change in their shape and orientation into account. For example, when applying deep-drawing operations (with triaxiality $\langle\bar{\sigma}\rangle > 0$) for manufacturing of axisymmetric case-shaped parts under large processing deformations it can happen that $\omega_1 < 1$ while $\omega_2 = 1$. *In this case using only one measure* (ω_1 *or* f_v) *for calculations would indicate non-criticality of damage while the second measure* ($\omega_2 = 1$) *reveals a critical stage of voids coalescence and generation of cavities.* This situation is undesirable or even unacceptable when producing metalware to be operated under intense loading and thermal actions which is widespread in aerospace, automotive, and energy engineering.

It should be noted once again that a successful practical application of the tensor theory to modeling of MF processes requires rather laborious experimental research on damage kinetics for deformed materials under complex loading. Such experiments will promote the creation of a database for meso-structural properties of plastically deformed materials which is necessary for computer simulations. To this end the authors have already begun their experimental research on the growth, shape change, and coalescence of meso-defects during stepwise plastic deformation of some structural metals. Tensile tests of sheet Al specimens with mock voids (pre-machined micro-holes) gave the following results: Voids take on a precise ellipsoidal shape elongated in the line of the principal strain axis (cf., Fig. 7). The strain $\widehat{\varepsilon}_{\text{void}}$ of ellipsoidal voids is appreciably larger than the strain ε_{RVE} of the material element (RVE) containing these imitation defects: $\widehat{\varepsilon}_{\text{void}}/\varepsilon_{\text{RVE}} \approx 1.4 - 1.5$. It could be verified that large imitation voids are the sources of localized strain bands which propagate in the direction of 55–60° to the axis of elongation. The commercial FE code ABAQUS was applied for processing the obtained experimental data on damage of strained materials. An example of FE calculations of equivalent plastic strains during uniaxial tension of the sheet Al specimen with imitation meso-defects is presented in Fig. 7. Such experimental data obtained for various types of the stress-strain state will allow us to realize a comparative assessment of different models of ductile damage in the near future.

In a single paper it is obviously impossible to discuss (even in a compressed form) all the questions pertinent to the presented physico-mechanical approach. The enhanced slip line method was used here in order to obtain the rapid and accurate solution of the applied problem. In future work the authors aim at coupling the constitutive equations of their tensorial theory with FE codes for MF processes.

Acknowledgments The present work was supported by Deutsche Forschungsgemeinschaft (DFG) by a special program for funding research stays in Germany of researchers from Central and Eastern Europe/CIS. This work was also supported by the President Grant for Young Russian Scientists and Their Advisers MK-4126.2006.8, and the Grant of the Albany-Tula Alliance, Inc. (A Restricted Gift from Prof. Charlotte S. Buchanan).

References

1. Bogatov, A.A., Mizhiritskiy, O.I., Smirnov, S.V.: Resource of Metals Plasticity during Forming. Metallurgy, Moscow (1984) (in Russian)
2. Bunge, H.J., Puhlandt, K., Tekkaya, A.E., Banabic, D.: Formability of Metallic Materials. Springer, Heidelberg (2000)
3. Gurson, L.: Continuum theory of ductile rupture by void nucleation and growth. J. Eng. Mater. Technol. Trans. ASME **99**, 2–15 (1977)
4. Horstemeyer, M.F., Matalanis, M.M., Sieber, A.M., Botos, M.L.: Micromechanical finite element calculations of temperature and void configuration effects on void growth and coalescence. Int. J. Plast. **16**, 979–1015 (2000)
5. Iljushin, A.A.: Plasticity: Fundamentals of the General Mathematical Theory. Nauka, Moscow (1963) (in Russian)
6. Kachanov, L.M.: Introduction to Continuum Damage Mechanics. Kluwer Academic, Dordrecht (1986)
7. Kachanov, L.M.: Fundamentals of the Theory of Plasticity. Dover Publications, New York (2004)
8. Klöcker, H., Tvergaard, V.: Growth and coalescence of non-spherical voids in metals deformed at elevated temperature. Int. J. Mech. Sci. **45**, 1283–1308 (2003)
9. Korn, G.A., Korn, T.M.: Mathematical Handbook for Scientists and Engineers: Definitions, Theorems, and Formulas for Reference and Review, 2nd revised edition. Dover Publications, New York (2000)
10. Krajcinovic, D.: Damage mechanics: accomplishments, trends and needs. Int. J. Solids Struct. **37**, 267–277 (2000)
11. Lemaitre, J., Desmorat, R.: Engineering Damage Mechanics: Ductile, Creep, Fatigue and Brittle Failures. Springer, Heidelberg (2007)
12. McClintock, F.A.: A criterion for ductile fracture by the growth of holes. J. Appl. Mech. **90**, 363–371 (1968)
13. Rice, J., Tracey, D.: On ductile enlargement of voids in triaxial stress field. J. Mech. Phys. Solids **17**, 201–217 (1969)
14. Sedov, L.I.: Continuum Mechanics, vol. 1. Nauka, Moscow (1983) (in Russian)
15. Sluzalec, A.: Theory of Metal Forming Plasticity. Springer, Heidelberg (2004)
16. Tutyshkin, N.D., Zapara, M.A.: The advanced method of definition of stress and velocity fields in the processes of axisymmetric plastic yielding. WSEAS Trans. Heat Mass Transf. **2**, 150–156 (2006)
17. Tutyshkin, N.D., Gvozdev, A.E., Tregubov, V.I.: Complex Problems of Plasticity Theory. Tul'skiy Polygraphist Publ., Tula (2001) (in Russian)
18. Tschaetsch, H.: Metal Forming Practise. Springer, Heidelberg (2006)
19. Voyiadjis, G.Z., Kattan, P.I.: Advances in Damage Mechanics: Metals and Metal Matrix Composites with an Introduction to Fabric Tensors, 2nd edn. Elsevier, Amsterdam (2006)
20. Yokobori, T.: An Interdisciplinary Approach to Fracture and Strength of Solids. Wolters-Noordhoff Scientific Publications Ltd., Groningen (1966)
21. Zapara, M.A., Tutyshkin, N.D., Müller, W.H., Weinberg, K., Wille, R.: A physicomechanical approach to modeling of metal forming processes—part I: theoretical framework. Continuum Mech. Thermodyn. **20**(4), 231–254 (2008)